Study of the relationship between electrical and magnetic properties and Jahn–Teller distortion in $R_{0.7}Ca_{0.3}Mn_{0.95}Fe_{0.05}O_3$ perovskites

2009 J. Phys.: Condens. Matter 21 026003

(http://iopscience.iop.org/0953-8984/21/2/026003)

J. Phys.: Condens. Matter **21** (2009) 026003 (5pp) doi:10.1088/0953-8984/21/2/026003

Study of the relationship between electrical and magnetic properties and Jahn–Teller distortion in $R_{0.7}Ca_{0.3}Mn_{0.95}Fe_{0.05}O_3$ perovskites

E K Abdel-Khalek[1], **W M EL-Meligy, E A Mohamed, T Z Amer and H A Sallam**

Physics Department, Faculty of Science, Al Azhar University, Nasr City, Cairo, Egypt

E-mail: eid_khalaf0@yahoo.com

Received 7 August 2008, in final form 28 October 2008
Published 9 December 2008
Online at stacks.iop.org/JPhysCM/21/026003

Abstract

In this work structural, magnetic and electrical properties of $R_{0.7}Ca_{0.3}Mn_{0.95}Fe_{0.05}O_3$ (R = Pr and Nd) perovskite manganites are presented. Structural characterization of these compounds shows that both have orthorhombic (*Pbnm*) phase. The Mössbauer spectra show clear evidence of the local structural distortion of the $Mn(Fe)O_6$ octahedron on the basis of non-zero nuclear quadrupole interactions for high-spin Fe^{3+} ions. It was found that the local structural distortion decreases significantly on replacing Pr^{3+} by Nd^{3+}. This replacement dependence of the Jahn–Teller coupling strength estimated from the Mössbauer results was found to be consistent with the electrical and magnetic properties.

(Some figures in this article are in colour only in the electronic version)

1. Introduction

Rare-earth manganite perovskites have been extensively studied because of their interesting electrical and magnetic properties [1, 2]. The substitution of rare-earth site with ones of smaller radii is expected to enhance the microstructural inhomogeneity, that may play an important role in the electrical and magnetic properties of the perovskite. One of the factors that are thought to be responsible for the variations is the structure tuning induced by the small ionic radius of the interpolated cation in the R site. Another one is the magnetic ionic characteristic of each rare earth. Early studies have shown that Mn^{3+} ions are mainly replaced by Fe^{3+} ions in this Fe-doping range, and that both ions have identical ionic radii in sixfold octahedral coordination [3, 4]. Therefore, the substitution of Fe^{3+} for Mn^{3+} does not change the structure and, consequently, the Jahn–Teller effect can be investigated from the quadrupole interaction of the Fe nucleus, although the Fe^{3+} ion is not a Jahn–Teller one [5]. Thus it can be assumed that the values of the second-order crystal electric field (CEF) coefficients for FeO_6 and MnO_6 octahedra are approximately the same in these compounds. Therefore, a few per cent of Fe, which substitutes for Mn in $R_{0.7}Ca_{0.3}Mn_{0.95}Fe_{0.05}O_3$ compounds, can be used as a micro-probe to detect the symmetry of the nearest-neighbor O^{2-} ions in the $Mn(Fe)O_6$ octahedron and its influence on the magnetic and electric properties.

2. Experimental details

The $R_{0.7}Ca_{0.3}Mn_{0.95}Fe_{0.05}O_3$ (R = Pr and Nd) perovskites were prepared by the co-precipitation method [6]. Powder x-ray diffraction (XRD) data of the samples were obtained at room temperature (RT) from a Siemens D5000 diffractometer using Cu Kα radiation. Rietveld analysis of the diffraction data was performed using the FULLPROF program. The size of the crystallographic grain has been deduced by applying the Scherrer formula [7]. The Mössbauer absorption spectra were recorded at RT using a conventional constant acceleration spectrometer with a ^{57}Co (Cr) radioactive source and using a metal Fe foil for calibration. The dc resistivity of the samples

[1] Author to whom any correspondence should be addressed.

Table 1. Structure parameters for RE^{3+} samples.

RE^{3+}	Pr^{3+}	Nd^{3+}
Lattice parameters	$a = 5.356$ $b = 5.355$ $c = 7.530$	$a = 5.350$ $b = 5.345$ $c = 7.525$
V (Å^3)	216.01	215.26
⟨Mn–O–Mn⟩ (deg)	130.43	132.38
⟨Mn–O⟩ (Å)	1.997	1.965
Cry size L (nm)	80.05	81.02

was measured by the conventional four-probe method in the temperature range 77–294 K. B–H curves were measured with a vibrating sample magnetometer (VSM) at 77 K.

3. Results and discussion

3.1. X-ray measurements

The x-ray diffraction (XRD) patterns for polycrystalline samples show that they are of single phase. Structural investigations using the standard Rietveld profile refinement showed that the synthesized samples crystallized in the distorted orthorhombic perovskite structure with space group $Pbnm$. From table 1 it is noticed that the lattice parameters decrease with replacement of Pr^{3+} ions by the smaller Nd^{3+} ions. This can be attributed to the decrease of the average ionic radius $\langle r_A \rangle$ where the octahedral tilt and rotate to reduce the excess space around the A site, leading to the decrease of the distances between two Mn ions as well as the decrease of unit cell volume [8]. The orthorhombic phase presents a ratio $c/a < \sqrt{2}$ characteristic of a cooperative Jahn–Teller deformation [9]. There is one long Mn–O bond and two short ones in the orthorhombic MnO_6 octahedra, which also reveal the presence of the Jahn–Teller distortion. The increase in particle size with the replacement of Pr^{3+} ions by smaller Nd^{3+} ions can be attributed to the decrease of the average ionic radius $\langle r_A \rangle$ and unit cell volume [10].

3.2. Mössbauer measurements

Mössbauer spectra for the $R_{0.7}Ca_{0.3}Mn_{0.95}Fe_{0.05}O_3$ manganite at room temperature consist of a single unresolved quadrupole doublet (figure 1) with isomer shift (IS) value (table 2) corresponding to Fe^{3+} cations in high-spin state located in the oxygen octahedral surrounding [11]. Hyperfine parameters are listed in table 2. The small values of the quadrupole splitting (QS) indicate the orthorhombic distortion of the ideal cubic perovskite structure [12].

The broadening in the line width (table 2) for the samples may be due to various reasons. The most common are superparamagnetic behavior due to nanocrystallite size and local environment effects [13]. The decrease of the QS value of Fe^{3+} ions on replacing Pr with Nd can be attributed to the increase of the ⟨Mn–O–Mn⟩. The decrease of the IS value of Fe^{3+} ions on replacing Pr with Nd can be attributed to the decrease in the Mn/Fe–O bond length as observed from the XRD results. The Jahn–Teller effect can be investigated directly from the obtained QS-values.

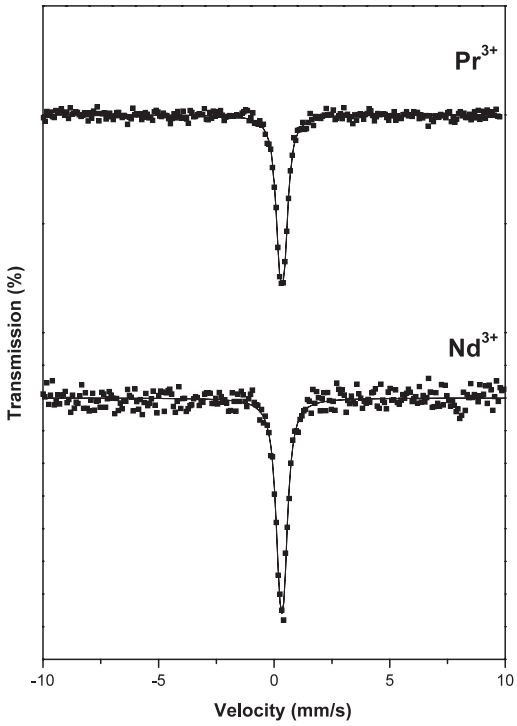

Figure 1. The Mössbauer spectra for the different RE^{3+} recorded at room temperature (RT).

Table 2. Mössbauer parameters as a function of the RE^{3+} content. (Note: QS is quadrupole splitting (mm s^{-1}); IS is isomer shift relative to Fe at room temperature (mm s^{-1}); LW is line width and E_{JT} is the Jahn–Teller coupling.)

RE^{3+}	QS (mm s^{-1})	IS (mm s^{-1})	LW (mm s^{-1})	E_{JT} (eV)
Pr^{3+}	0.21	0.34	0.41	0.73
Nd^{3+}	0.18	0.33	0.44	0.64

The local structural distortion of MnO_6 octahedra resulting from the Jahn–Teller effect of high-spin Mn^{3+} ions removes the degeneracy of the e_g and t_{2g} orbitals so as to make some energy levels more stable. The e_g orbital group is separated into two energy levels, d_{z^2} and $d_{x^2-y^2}$. The energy separation of the upper-level orbitals e_g has been shown to be larger than that of the lower-level orbitals. Since the Jahn–Teller distortion strongly influences the electron hopping process between the upper-level orbitals of Mn^{3+} and Mn^{4+} ions in $R_{0.7}Ca_{0.3}Mn_{0.95}Fe_{0.05}O_3$ perovskites, and consequently determines the ferromagnetic and electrical behaviors, we only need to consider the upper-level splitting of e_g orbitals. It has been pointed out in [14] that the energy separation between d_{z^2} and $d_{x^2-y^2}$ orbitals arises mainly from the contribution of the second-order crystal electric field (CEF) coefficient of the distorted MnO_6 octahedra, $A_{20}(MnO_6)$, and that the relationship between the Jahn–Teller coupling, E_{JT}, and $A_{20}(MnO_6)$ can be written as

$$E_{JT} = \frac{2e}{7}\sqrt{\frac{5}{\pi}} A_{20}(MnO_6) \langle r^2 \rangle_{Mn},$$

where $\langle r^2 \rangle$ is the expectation value of the square of the radial distance of the Mn^{3+} ion 3d orbital from the nucleus.

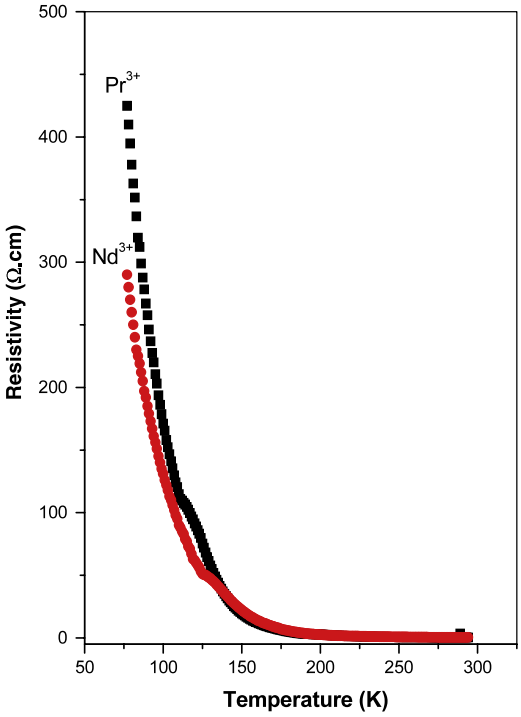

Figure 2. Temperature dependence of resistivity for different RE^{3+}.

Mössbauer spectroscopy can be employed to determine the value of A_{20} by a measurement of the quadrupole splitting, as described below. Since the QS at the nucleus of an Fe^{3+} ion is solely the result of contributions from the surrounding ions, the value of $A_{20}(FeO_6)$ can be obtained from

$$A_{20}(FeO_6) = \sqrt{\frac{4\pi}{5}}\frac{\Delta(Fe^{3+})}{eQ[1+\frac{\eta^2}{3}]^{1/2}},$$

where Q is the electric quadrupole moment of the ^{57}Fe nucleus and η is the asymmetry parameter. Since the Mn^{3+} and Fe^{3+} ions have identical ionic radii (0.645 Å) in sixfold octahedral coordination [4], it is assumed that $A_{20}(MnO_6) \approx A_{20}(FeO_6)$. Therefore, the relationship between E_{JT} and the quadrupole splitting at the Fe^{3+} ion, Δ (Fe^{3+}), can be written as

$$E_{JT} = \frac{4\Delta(Fe^{3+})}{7Q[1+\frac{\eta^2}{3}]^{1/2}}\langle r^2\rangle_{Mn}.$$

The quadrupole splitting for the Mössbauer experiment is generally in units of mm s^{-1}. Here it should be converted to eV by a factor of $E\gamma/c$, where $E\gamma = 14.4$ keV for the $I = 3/2 \leftrightarrow 1/2$ transition of ^{57}Fe and $c = 3\times10^{11}$ mm s^{-1} is the velocity of light [14]. In the case of axial symmetry, $\eta = 0$. Using approximately the expectation value $\langle r^2\rangle$ of free Mn^{3+} ions, $\langle r^2\rangle = 0.3535$ $Å^2$, and $Q = 0.28\times10^{-24}$ cm^2 [15], the Jahn–Teller coupling, E_{JT}, in each perovskite was estimated (table 2). From table 2, it is found that the energy separation between d_{z^2} and $d_{x^2-y^2}$ decreases with replacement of Pr^{3+} ions by smaller Nd^{3+} ions. This can be attributed to the decrease of local structural distortion which is due to the increase of the ⟨Mn–O–Mn⟩.

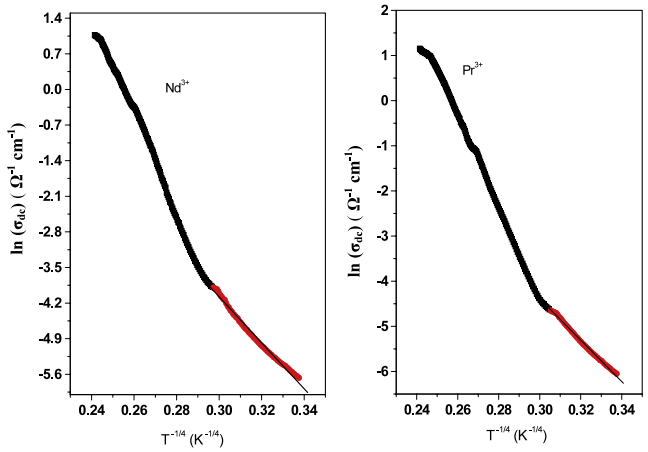

Figure 3. Plot of $\ln(\sigma)$ versus $T^{-1/4}$; the solid line indicates the best fit for the VRH model equation.

3.3. Electric measurements

The results of the resistivity versus temperature of the samples in zero magnetic field are illustrated in figure 2. All samples behave as semiconductors in the whole temperature range studied. The absence of a metal–semiconductor transition is attributed to the grain boundary effect due to nanocrystallites and the small kink in the resistivity of the samples is due to the structural transition [16]. From figure 2 it can be seen that the electrical resistivity decreased with replacement of Pr^{3+} ions by the smaller Nd^{3+} ions especially at low temperatures. This may be due to the increase of the Mn–O–Mn bond angle and the decrease of the Mn–O distance, then the overlap between the relevant orbitals is better, and the probability of hopping occurring higher.

In order to explain the electronic conduction, two models, namely the variable range hopping model (VRH) of charge carriers ($T < \theta_D/2$, where θ_D is Debye temperature) and the small polaron hopping ($T > \theta_D/2$), are generally used. The VRH in three-dimensional cases can be written as [17, 18] $\sigma_{dc} = \sigma_0\exp[-(T_0/T)]^{1/4}$, where σ_0 is a pre-exponential factor, T_0 is a constant ($T_0 = 16\alpha^3/k_BN(E_F)$), α is the electron wavefunction decay constant, k_B is Boltzmann's constant and $N(E_F)$ is the density of states at the Fermi level, which can be calculated from the slope of the plot of the $\ln(\sigma_{dc})$ versus $T^{-1/4}$ curve (shown in figure 3). From the best fits $\theta_D/2$ values are estimated. Here, half the θ_D is defined as the temperature at which deviation from linearity occurs in the temperature region (figure 3). Further T_0 values for each sample were calculated from slopes of the $\ln(\sigma)$ versus $T^{-1/4}$ plot. From the above equation we estimated $N(E_F)$ (table 3) using the value $\alpha = 2.22$ nm^{-1} used by Pal *et al* [19] and found it to be in agreement with those reported in the literature for other manganite materials [20], while the conduction mechanism of these materials at high temperatures ($T > \theta_D/2$) is governed by small polarons and the polaronic models could be due to either adiabatic or non-adiabatic approximations [21]. The temperature dependence of the electrical resistivity arising out of adiabatic and

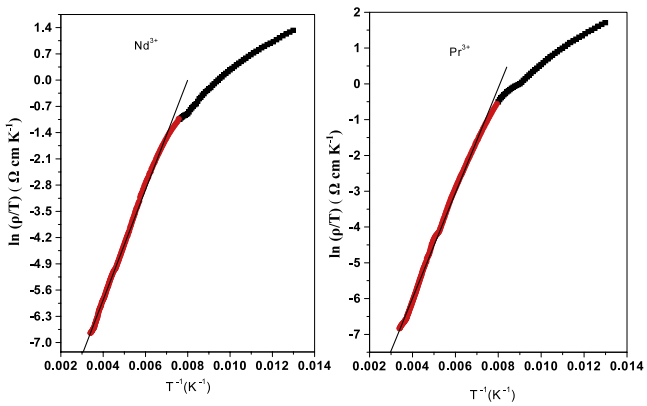

Figure 4. Plot of $\ln(\rho/T)$ versus T^{-1}; the solid line indicates the best fit for the equation $\rho = \rho_\alpha T \exp(E_p/K_B T)$.

Table 3. The best fit parameters obtained from the experimental resistivity data.

RE^{3+}	θ_D (K)	$N(E_F)$ (eV^{-1} cm^{-3})	T_0 (10^6 K)	E_p (meV)
Pr^{3+}	230	1.80×10^{16}	4.432	127.0
Nd^{3+}	258	1.90×10^{16}	4.180	126.4

non-adiabatic approximations is given by

$$\rho = \rho_\alpha T \exp(E_p/K_B T) \text{ (adiabatic)}$$

$$\rho = \rho_\alpha T^{3/2} \exp(E_p/K_B T) \text{ (non-adiabatic)},$$

where ρ_α is the residual resistivity, and E_p is the activation energy. According to Jung *et al* [22], higher values (two or three orders higher than those of the usual oxide semiconductors) of $N(E_F)$ in the present manganite system could be due to their high value of conductivity. These higher values of $N(E_F)$ are clear signatures of the applicability of the adiabatic hopping mechanism. Based on this fact, the adiabatic small polaron hopping model rather than the non-adiabatic small polaron hopping model can be used in the present investigation. We have replotted the resistivity curve as $\ln(\rho/T)$ versus $1/T$ (see figure 4), and from the slope of the curve the activation energy E_P is estimated (table 3). It can be seen from the table that the activation energy values are found to decrease and $N(E_F)$ increases with replacement of Pr^{3+} ions by the smaller Nd^{3+} ions. These results can be attributed to the increase of the Mn–O–Mn bond angles and the decrease of the Mn–O distance. In addition to the increase of the grain size, the observed behavior may be due to the fact that with increasing grain size interconnectivity between grains increases, which helps the conduction electron to hop to the neighboring sites [20]. This is consistent with the Jahn–Teller energy separation obtained from Mössbauer results.

3.4. Magnetic measurements

Figure 5 shows the variation in flux density (B) as a function of applied magnetic field (H) at 77 K. The shape of the hysteresis loop is characteristic of weak ferromagnetism. Even a field

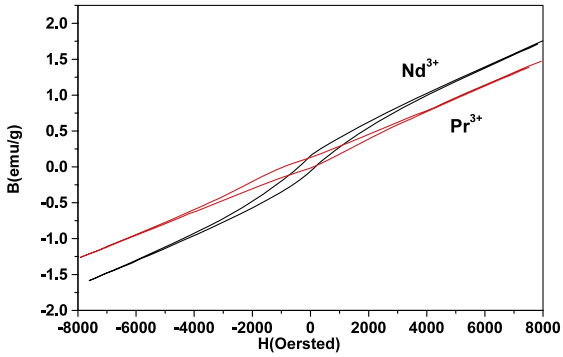

Figure 5. The magnetic hysteresis (B–H) measurements for the different RE^{3+} at 77 K.

Table 4. B_s, B_r and H_c for the different RE^{3+} contents.

RE^{3+}	B_s (emu g^{-1})	B_r (emu g^{-1})	H_c (Oe)
Pr^{3+}	1.367	0.074	510.1
Nd^{3+}	1.695	0.104	277.4

of 0.8 T does not saturate the hysteresis curve, and the flux density still has a tendency to increase, which is characteristic of the mainly antiferromagnetic ordering of the spins in the nanoparticles [10]. The saturation B_s is measured at $H = 0.8$ T and $T = 77$ K, coercive field H_C and remanent B_r are listed in table 4. It can be seen from the table that the saturation B values increase with replacement of Pr^{3+} ions by the smaller Nd^{3+} ions. This may be because the ferromagnetic (FM) contribution for the Nd sample is much higher than that of the Pr sample. The phenomenon is possibly due to the existence of field induced Nd moment, which interacts with the Mn moment and destabilizes the AFM structure, and leads to the development of FM double exchange interaction [23]. This is in agreement with the hypothesis previously proposed by Tokunaga *et al* [24] for $Nd_{0.5}Ca_{0.5}MnO_3$. While the decrease of coercive field can be attributed to the increase of the grain size for the polycrystalline ferromagnets, grain boundaries are magnetic domain boundaries. As the domain wall mobility is determined by the volume density of these defects, the coercive field decreases with increasing grain size in the following way [25]: $H_c = H_{c,o} + (K_M/D)$ where $H_{c,o}$ are reflects the coercivity due to other effects, such as internal stresses, impurities, etc, K_M is a constant and D is the grain size. The observed behavior may be explained following the work by Dutta *et al* [26]. According to these authors, the magnetic and transport properties of the perovskite manganites are strongly coupled and are very sensitive to Mn–O–Mn bond angle and Mn–O bond length. It has been found that for fine particle perovskite manganites, a decrease in magnetization and an increase in resistivity occur as we decrease the particle size, because of broken Mn–O–Mn bonds at the surface of the smaller particles that hamper exchange interaction and degrade connectivity for electron conduction, but here in this case it seems that the spin interaction increases and the connectivity improves as we increase the particle size. The increase in particle size results in an increase in Mn–O–Mn bond angle and

a decrease in Mn–O bond length. This is consistent with Jahn–Teller energy separation obtained from Mössbauer results.

4. Conclusions

Mössbauer results which show clear evidence of the local structural distortion of the $Mn(Fe)O_6$ octahedron can be effectively employed to estimate the Jahn–Teller coupling of these perovskites. The change of rare-earth site (Pr or Nd) dependence of the Jahn–Teller coupling strength estimated from the Mössbauer results was found to be consistent with the electric and magnetic properties. The variable range hopping and small polaron models results show that the changes in the behavior of the density of states at the Fermi level and activation energy with change of rare earth are in agreement with the change in the Jahn–Teller coupling energy. Consequently, the connection between the local structural distortion and the electrical and magnetic behavior of this material can be well explained.

Acknowledgment

The authors would like to thank Professor Said Farag Mostafa, Powder Technology Department, Central Metallurgical R&D Institute, El-Tebbin, Helwan, Cairo, Egypt, for providing the facility for the magnetic measurements.

References

[1] Helmolt R V, Wecker J, Holzapfel B, Schultz L and Samwer K 1993 *Phys. Rev. Lett.* **71** 2331
[2] Miao J H, Yuan S L, Ren G M, Xiao X, Yu G Q, Wang Y Q and Yin S Y 2007 *Mater. Sci. Eng.* B **136** 67
[3] Liu X J, Li Z Q, Wu P, Bai H L and Jiang E Y 2007 *Solid State Commun.* **142** 525
[4] Kou Z, Ma X, Di N, Li Q and Cheng Z 2005 *Phys. Status Solidi* b **242** 2930
[5] Wei L, Wang Y B, Wang H Y, Yue Y, Wang T M, Zhang T B and Cao G H 2000 *Chin. Phys. Lett.* **17** 446
[6] Vijayanandhini K and Kutty T R N 2007 *Solid State Commun.* **141** 252
[7] Banerjee A, Pal S, Bhattacharya S and Chaudhuri B K 2002 *J. Appl. Phys.* **91** 5125
[8] Hannoyer B, Marest G, Greneche J M, Bathe R, Patil S I and Ogale S B 2000 *Phys. Rev.* B **61** 9613
[9] Dhahri R and Halouni F 2004 *J. Alloys Compounds* **385** 48
[10] Li J, Xinli K, Yong Q and He H 2002 *Phys. Status Solidi* a **191** 255
[11] Kopcewicz M, Khomchenko V A, Troyanchuk I O and Szymczak H 2004 *J. Phys.: Condens. Matter* **16** 4335
[12] Simopoulos A, Pissas M, Kallias G, Devlim E, Moutis N, Panagiotopoulos I, Niarchos D, Christides C and Sonntag R 1999 *Phys. Rev.* B **59** 1263
[13] Mostafa A G, Abdel-Khalek E K, Daoush W M and Moustfa S F 2008 *J. Magn. Magn. Mater.* **320** 3356–60
[14] Cheng H, Wang Z H, Di N L, Kou Z Q, Wang G J, Li R W, Lu Y, Li Q A, Shen B G and Dunlap R A 2003 *Appl. Phys. Lett.* **83** 1587
[15] Miao J H, Yuan S L, Ren G M, Xiao X, Yu G Q, Wang Y Q and Yin S Y 2007 *Mater. Sci. Eng.* B **136** 67
[16] Urushibara A, Moritomo Y, Arima T, Asamitsu A, Kido G and Tokura Y 1995 *Phys. Rev.* B **51** 14103
[17] Mollah S, Huang H L, Yang H D, Pal S, Taran S and Chaudhuri B K 2004 *J. Magn. Magn. Mater.* **284** 383
[18] Mott N F and Davis E A 1979 *Electronics Process in Non Crystalline Materials* (Oxford: Clarendon)
[19] Pal S, Banerjee A, Rozenberg E and Chaudhuri B K 2001 *J. Appl. Phys.* **89** 4955
[20] Venkataiah G and Venugopal Reddy P 2005 *J. Magn. Magn. Mater.* **285** 343
[21] Emin D and Holstein T 1969 *Ann. Phys.* **53** 439
[22] Jung W H 1998 *J. Mater. Sci. Lett.* **17** 1317
[23] Zhu D, Cao P, Liu W, Ma X, Maignan A and Raveau B 2007 *Mater. Lett.* **61** 617
[24] Tokunaga M, Miura N, Tomioka Y and Tokura Y 1998 *Phys. Rev.* B **57** 5259
[25] Artz E 1998 *Acta Mater.* **46** 5611
[26] Dutta A, Gayathri N and Ranganathan R 2003 *Phys. Rev.* B **68** 054432